# Wavefront healing operators for improving reflection coherence

David C. Henley

## ABSTRACT

Seismic reflection image continuity is often adversely affected by inadequate acquisition or processing procedures, by the interference of various kinds of noise, or by the irregular nature of the recording surface. In situations where conventional methods fail, a simple processing technique called "wavefront healing" can increase reflection continuity enough to significantly improve the interpretation. The operation can be applied to either trace gathers or stacked sections. Two different operators based on the Huygens wavelet construction model of seismic wavefront propagation have been implemented in ProMAX at CREWES and are demonstrated here on both real and model data.

## INTRODUCTION

Sometimes, in spite of best efforts, satisfactory images of seismic reflectors cannot be obtained by conventional means. One of the more common causes of this situation is the presence of irregularities in the earth just beneath the surface. Even if a seismic wavefront returns to the vicinity of the surface as a relatively coherent reflected event, it may be disrupted by traversing the last few metres to the surface, when the near-surface material is irregular or rests on a rugged bedrock surface. This causes static delays in small portions of a returning wavefront as well as scattering and mode conversions from discontinuities in the earth materials. As a result, the wavefront image exhibits short-wavelength static jitter and amplitude fluctuations due to interference by various noises. Figure 1 portrays this disruption schematically.

Diffractions on seismic sections are familiar to geophysicists and indicate the need to "migrate" the data to remove the smoothing effects of the physical wavefronts from the reflection images. Less familiar is the idea of deliberately introducing diffraction into image processing. Huygens wavelet construction is a historical geometrical technique, based on diffraction, for propagating reflection images on time sections. It can also be used to introduce the smoothing effects of diffraction into reflection images. A diffraction results physically whenever the local curvature of an interface exceeds the curvature of an incident wavefront. Consequently, Huygens wavelet construction, using wavelets with curvature smaller than that of reflection image irregularities, can be used to propagate reflection images and smooth them simultaneously. Physically, the process simulates burying the earth's surface beneath a layer of uniform material and recording a wavefront after it propagates to the new surface via wavelets originating at points coincident with receiver locations on the original surface, the wavefront being smoothed or 'healed' by its transit. The actual recording surface can't be moved after the data are recorded, but the surface can be *effectively* moved further away during processing using the Huygens wavelet construction in a simple processing algorithm. The technique described is similar to

wave equation datuming (Berryhill, 1979), (Yang, 1999), or to modelling by demigration (Jaramillo et al, 1997), (Jaramillo et al, 1999), but is simpler than either.

To propagate a reflection image with Huygens wavelets, a velocity is chosen (which determines the wavelet radius, curvature and propagation time), and circular wavelets are constructed using closely spaced points on the reflection image as origins of different wavelets of the same radius (see Figure 1). The envelope (summation) of the resulting wavelet amplitudes, in the direction of propagation, forms the propagated image of the reflection. The reflection image increases in smoothness and coherence with each propagation step, depending directly upon the chosen propagation velocity. Figure 2 shows the interface in Figure 1 after two steps of Huygens wavelet propagation. The increased smoothness with respect to the distorting interface is significant. This heuristic model, then, is the basis for a pair of processing operations called "wavefront healing", as detailed and shown below.

## ALGORITHM DETAILS

Wavefield images in digital seismic data are not by nature continuous, but are discretised using grids defined by traces and time samples. The wavefront healing algorithm is constrained by this fundamental sampling; its step size and wavelet radius tied in a basic way to the sample increment in both the X and T dimensions. Each of the algorithms described here has been organised as a 'gathering' operation, in which a selected output point is the sum of vector amplitudes from all points at a constant (earlier) delay time on a Huygens wavelet surface centred on the output point. In the three-point algorithm, each trace takes amplitudes only from itself and its two nearest neighbour traces) to compute output, while in the five-point algorithm, amplitudes are also used from the next-nearest neighbour traces. The Huygens construction for the three-point algorithm, and the relationships between various distances and delay times is shown in Figure 3, while the discrete formula is expressed in equation 1:

$$
\begin{aligned}
A(n, T + d) = W\{ & A(n, T) \\
& + \cos(\alpha_l)\left[(t_{dl}/d)A(n-1, T+d) + (t_{vl}/d)A(n-1, T)\right] \\
& + \cos(\alpha_r)\left[(t_{dr}/d)A(n+1, T+d) + (t_{vr}/d)A(n+1, T)\right] \} \; ;
\end{aligned}
\tag{1}
$$

$$
\cos(\alpha_l) = t_{vl}/t_r, \qquad\qquad \cos(\alpha_r) = t_{vr}/t_r,
$$

$$
t_{vl} = \sqrt{t_r^2 - t_{hl}^2}\;, \qquad\qquad t_{vr} = \sqrt{t_r^2 - t_{hr}^2}\;,
$$

$$
t_{hl} = \left[x(n) - x(n-1)\right]/v, \qquad t_{hr} = \left[x(n+1) - x(n)\right]/v,
$$

$$
t_{dl} = d - t_{vl}, \qquad t_{dr} = d - t_{vr}, \qquad t_r = d, \qquad W = 1/\left[1 + \cos(\alpha_l) + \cos(\alpha_r)\right],
$$

where $A(n,T)$ is the wavefield amplitude on trace $n$ at time $T$; $d$ is the sample interval; $x(n)$ is the source-receiver offset of trace $n$; $t_{hl}$, $t_{hr}$ are horizontal delay times between points identified in Figure 3; $t_{vl}$, $t_{vr}$, $t_{dl}$, $t_{dr}$ are vertical delay times between points identified in Figure 3; $t_r$ is the Huygens radius; $v$ is the propagation velocity; and $W$ normalises the vector summation with respect to unity.

The details for the five-point wavefront healing algorithm are illustrated in Figure 4 and the discrete formula is given in equation 2:

$$A(n,T+2d) = W \{ A(n,T)$$
$$+ \cos(\alpha_{l1})[(t_{dl1}/d)A(n-1,T+d) + (t_{vl1}/d)A(n-1,T)]$$
$$+ \cos(\alpha_{l2})[(t_{dl2}/d)A(n-2,T+2d) + (t_{vl2}/d)A(n-2,T+d)]$$
$$+ \cos(\alpha_{r1})[(t_{dr1}/d)A(n+1,T+d) + (t_{vr1}/d)A(n+1,T)]$$
$$+ \cos(\alpha_{r2})[(t_{dr2}/d)A(n+2,T+2d) + (t_{vr2}/d)A(n+2,T+d)]\} ; \qquad (2)$$

$$\cos(\alpha_{l1}) = (t_{vl1}+d)/t_r , \qquad \cos(\alpha_{r1}) = (t_{vr1}+d)/t_r ,$$

$$\cos(\alpha_{l2}) = t_{vl2}/t_r , \qquad \cos(\alpha_{r2}) = t_{vr2}/t_r ,$$

$$t_{vl1} = \sqrt{t_r^2 - t_{hl1}^2} - d , \qquad t_{vr1} = \sqrt{t_r^2 - t_{hr1}^2} - d ,$$

$$t_{vl2} = \sqrt{t_r^2 - t_{hl2}^2} , \qquad t_{vr2} = \sqrt{t_r^2 - t_{hr2}^2} ,$$

$$t_{hl1} = [x(n) - x(n-1)]/v , \qquad t_{hr1} = [x(n+1) - x(n)]/v ,$$

$$t_{hl2} = [x(n) - x(n-2)]/v , \qquad t_{vr2} = [x(n+2) - x(n)]/v ,$$

$$t_{dl1} = d - t_{vl1} , \qquad t_{dr1} = d - t_{vr1} ,$$

$$t_{dl2} = d - t_{vl2} , \qquad t_{dr2} = d - t_{vr2} ,$$

$$t_r = 2d , \qquad W = 1/[1 + \cos(\alpha_{l1}) + \cos(\alpha_{l2}) + \cos(\alpha_{r1}) + \cos(\alpha_{r2})],$$

where $A(n,T)$ is the wavefield amplitude on trace $n$ at time $T$; $d$ is the sample interval; $x(n)$ is the source-receiver offset of trace $n$; $t_{hli}$, $t_{hri}$, $_{i=1,2}$ are horizontal delay times between points identified in Figure 4; $t_{vli}$, $t_{vri}$, $t_{dli}$, $t_{dri}$, $_{i=1,2}$ are vertical delay times between points identified in Figure 4; $t_r$ is the Huygens radius; $v$ is the propagation velocity; and $W$ normalises the vector summation with respect to unity.

The choice of propagation velocity, as well as the X co-ordinates of the traces determines the radius of the wavelet, and hence the intersections of the wavefront with the traces. Either algorithm chooses the minimum radius that will force the wavelet to intersect both nearest neighbour traces (and next-nearest traces in the case of the five-point algorithm) and thus include their amplitudes. The output of the

healing operator consists of a vector sum of all trace amplitudes intersected by the wavelet, assigned to the point at the origin of the wavelet. The vector sum requires that trace amplitudes are weighted by the cosine of their incidence angle with respect to the wavelet origin. This particular implementation of wavefront healing is appropriate for land seismic data, in which particle velocity or acceleration vectors are the usual seismic measurements, but not for pressure scalar measurements, which occur in marine data.

Although both wavefront healing algorithms are designed for uniformly gridded data, they can accommodate irregular offset spacing on the trace gathers to which they are applied. Time delays, cosine weights, and interpolation weights all depend upon specific source-receiver offsets, and are computed individually for each trace. Also, though intended primarily for 'upward continuation', in which events are propagated to greater time as they heal, both modules have the option to run in reverse 'downward continuation' mode. The former is quite similar to a local "de-migration", while the latter has no particular physical analogy and thus not much actual justification for use, except that it improves reflection continuity.

Like many grid-based techniques, wavefront healing is subject to stability constraints related to the sampling interval in both dimensions of the input data. Specifically, the velocity chosen for the wavelet should be large enough that the product of velocity and time sample increment exceeds the nominal distance increment between traces. When the velocity is lower than this stability criterion, aliasing and dispersion will occur and become apparent after more than one or two steps of healing. Because wavefront curvature is inversely proportional to velocity, very large velocity values cause wavefront healing to approach lateral trace-mixing in its effects. Another effect associated with wavefront healing is the loss of higher frequencies from reflection events being healed, the loss being greatest for low velocities. Since these techniques are intended only for application to data with very poor coherent signal-to-noise ratio, some loss of energy at higher frequencies may well be acceptable in order to enhance overall event coherence.

## SOFTWARE

The wavefront healing operators described above in equations (1) and (2) and Figures 3 and 4 have been implemented as ProMAX operations called "Wavefront healing" and "Wavefront healing II", respectively, where the latter is the five-point algorithm. Both modules are included in the 2000 CREWES software release and are fully documented in the help files. The parameters, of which there are only three, are the same for either module. Specifically, the first parameter is the propagation velocity to be used for the Huygens wavelet construction, the second is the number of propagation steps to apply, and the third is simply the choice of upward (default) or downward continuation. The latter term may cause some confusion, although used here in the conventional sense, as upward continuation actually propagates the reflections *downward* (greater in time) on the section or gather.

# EXAMPLES

To demonstrate the action of wavefront healing on seismic traces, three synthetic examples are presented, followed by two field data examples. Figure 5 shows the three synthetic models built to illustrate the wavefront healing operations. Figure 5a is an isolated, bandlimited spike, useful for illustrating the wavefront healing operator 'impulse response'; Figure 5b is a simulated plane reflector with a gap; and Figure 5c is a simulated plane reflector with various 'static' displacements. The latter two models exhibit some of the kinds of event disturbances that wavefront healing is intended to address.

The three-point wavefront healing algorithm is illustrated first in Figure 6, where the operator has been applied for one step, and in Figure 7, where two steps of healing have been applied. A convenient way to think of the impulse responses in Figures 6a and 7a is as Huygens wavefronts propagating downward to greater time from a diffracting point. The spreading and smoothing action of the operator is readily evident not only in the impulse responses, but in the model reflection responses in Figures 6b, 6c, 7b, and 7c. Note, as well, that each step of healing shifts the reflection event to greater time. This simulates burying the old surface beneath a layer of uniform material and placing new detectors on top of the new layer.

Figures 8 and 9 feature the impulse and model responses for the five-point wavefront healing algorithm for one and two steps, respectively. It is obvious that this algorithm has roughly twice the smoothing action per step of the three-point algorithm for the same velocity. What may be less apparent, however, is the fact that the five-point algorithm also exhibits greater attenuation of high frequencies per step. Although not shown here, running either algorithm in the reverse direction (downward continuation instead of upward continuation) reverses the curvature of the impulse responses and shifts reflections to smaller time. The action of the algorithms is exactly the same in either direction.

To illustrate the action of wavefront healing on field data, a shot gather was selected from the Blackfoot 2-D 3-C survey of 1995, and is shown in Figure 10. This gather is relatively good quality data and would not ordinarily warrant the use of wavefront healing, although radial trace filtering *would* be considered. There are, however, enough disturbances of various kinds exhibited on the reflections to illustrate wavefront healing effectively. These include interfering patterns of coherent noise, random noise, small amounts of static jitter, a low level of random noise, a trace overwhelmed by 60 Hz hydro-line pickup, and a couple of traces consisting of high frequency random noise.

Figures 11a and b show the effect of applying one step of three-point and five-point wavefront healing, respectively, using a velocity of 3000 m/s. The direct arrival velocity was chosen, though a wide range of other velocities can be used. As can be seen in the figures, wavefront healing with either algorithm dramatically reduces trace-to-trace fluctuations along reflections, with the effect being greatest for the five-point algorithm, as expected.

Since wavefront healing can also be applied to stacked sections, a stack of the vertical component data from the Blackfoot survey is shown in Figure 12, while Figures 13a and b show the results of applying one step of wavefront healing for the 3-point and 5-point algorithms, respectively. As can be seen, wavefront healing acts as a very effective cleaning agent for residual noise, particularly noise which varies rapidly laterally.

## DISCUSSION

It is interesting to note that the action of wavefront healing is relatively gentle, although as demonstrated on the synthetic models, one or two steps of healing can have a significant effect on the appearance of a gather or section of real seismic data. A very good example of this is shown in an accompanying chapter (Henley, 2000), where two very marginal stacked sections have their lateral continuity dramatically improved by only one or two passes of the three-point wavefront healing algorithm. Furthermore, experience has shown that seismic data need not correspond to the model on which wavefront healing is based (emerging wavefronts disrupted by a rugged interface) in order to benefit from the technique. In fact, another situation that benefits from wavefront healing is interference by coherent noise, if the noise wavefronts slope significantly. Wavefront healing in this case propagates only the horizontal, vertically travelling wavefronts and attenuates the rest.

One side effect of wavefront healing that should be reiterated is the reduction in resolution in both X and T dimensions. Every individual set of data will be affected differently by wavefront healing, so each new set should be tested with an operator, trying different velocities and numbers of steps. In general, however, the wavefront healing operator increases lateral coherence at the expense of resolution in both dimensions. Higher propagation velocities lead to more lateral smearing and less bandwidth loss, while lower velocities lead to less lateral smearing but greater high frequency loss and sometimes causes aliasing, if the stability criterion has been violated. Finally, all effects of wavefront healing are cumulative—each healing step compounds the effects of previous steps, whether increased coherence or lost resolution.

## CONCLUSIONS

When conventional seismic acquisition and/or processing methods fail to provide seismic data of sufficient quality to form usable images, an unconventional technique like wavefront healing can sometimes be used to force a trade-off between event resolution and coherence, decreasing the former in favour of the latter. In particular, for very noisy data gathered with very high resolution (but sometimes low fold), wavefront healing can provide a way to make use of disappointing survey results.

## ACKNOWLEDGEMENTS

# REFERENCES

Berryhill, J.R., 1979, Wave equation datuming: Geophysics, **44**, no. 8, 1329-1344.

Henley, D.C., 2000, Harsh imaging techniques for shallow high resolution seismic data, CREWESresearch report **12.**

Jaramillo, H.H. and Bleistein, N., 1997, Demigration and migration in isotropic inhomogeneous media: Annual Meeting Abstracts, Society of Exploration Geophysicists, 1673-1676.

Jaramillo, H.H., and Bleistein, N., 1999, The link of Kirchhoff migration and demigration to Kirchhoff and Born modelling: Geophysics, **64**, no. 6, 1793-1805.

Yang, K., 1999, Wave equation datuming from irregular surface using finite-difference scheme: Annual Meeting Abstracts, Society of Exploration Geophysicists, 1465-1468.

**FIGURES**
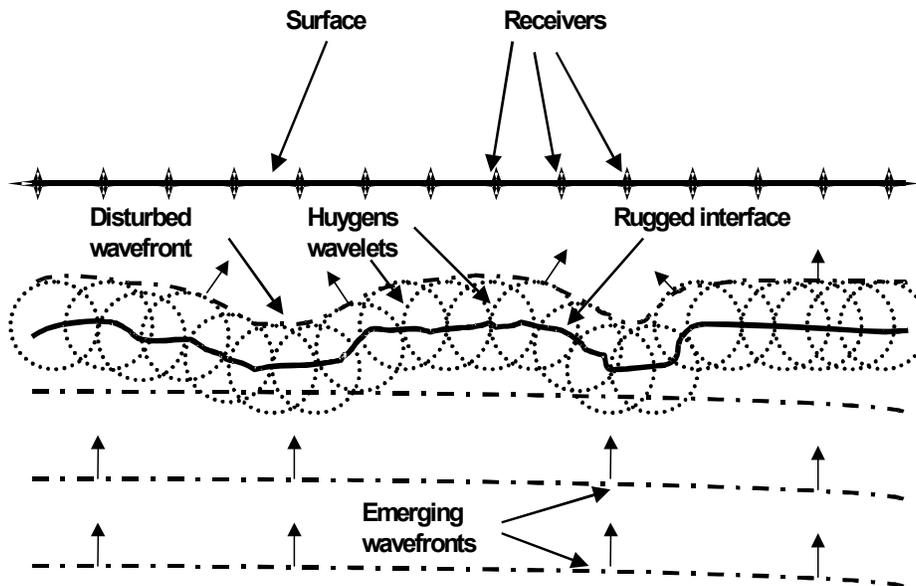


Figure 1. Coherent wavefronts from deep reflections being disrupted by passage through a rugged interface. Huygens wavelet construction illustrates how the disturbed wavefront can be constructed by considering the interface to be composed of point sources.
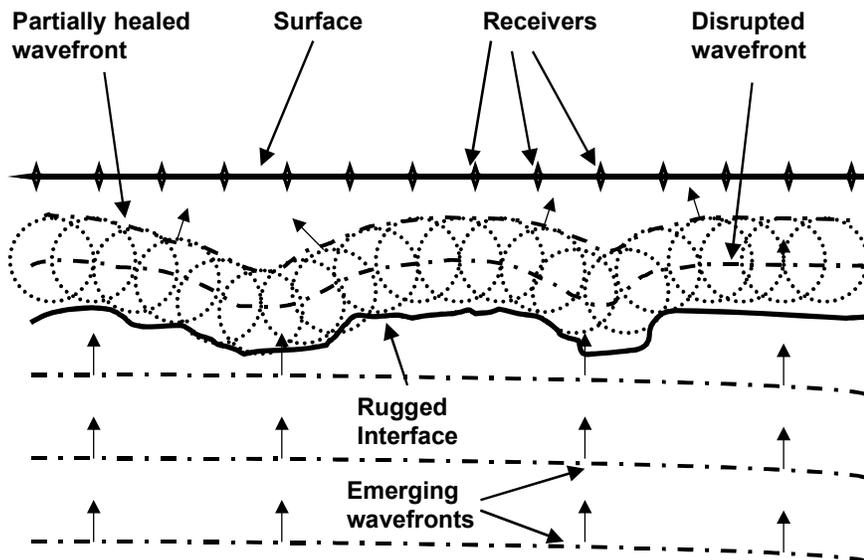


Figure 2. Disrupted wavefront after one further step of propagation. Huygens wavelet construction used to propagate disrupted wavefront from Figure 1 to the new position. Note the increased smoothness of the propagated wavefront.
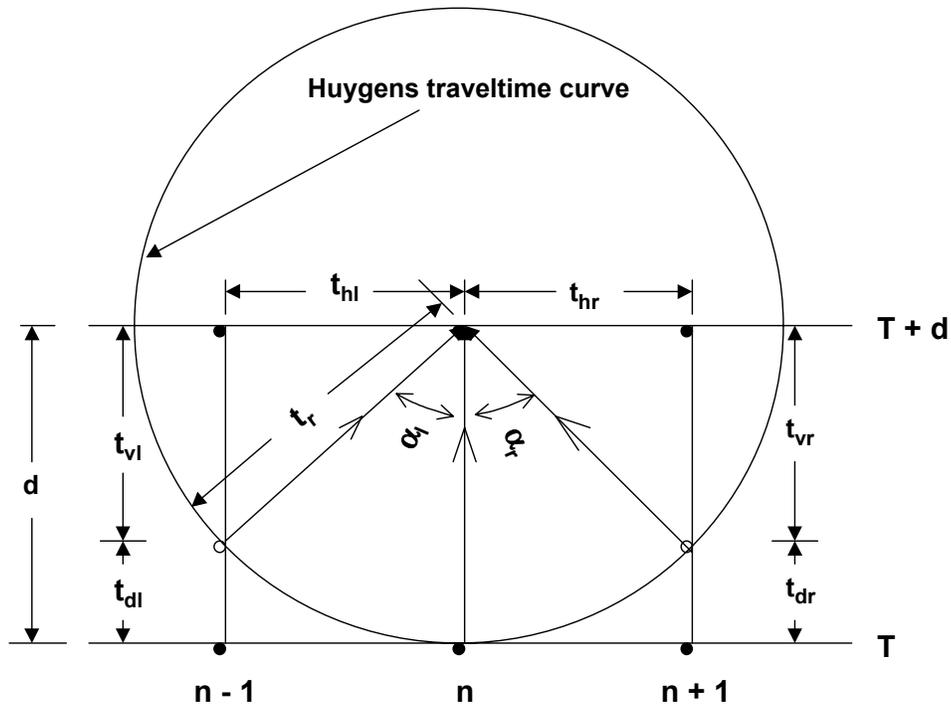
Figure 3. The various times and angles used in the three-point wavefront healing algorithm expressed in equation 1.
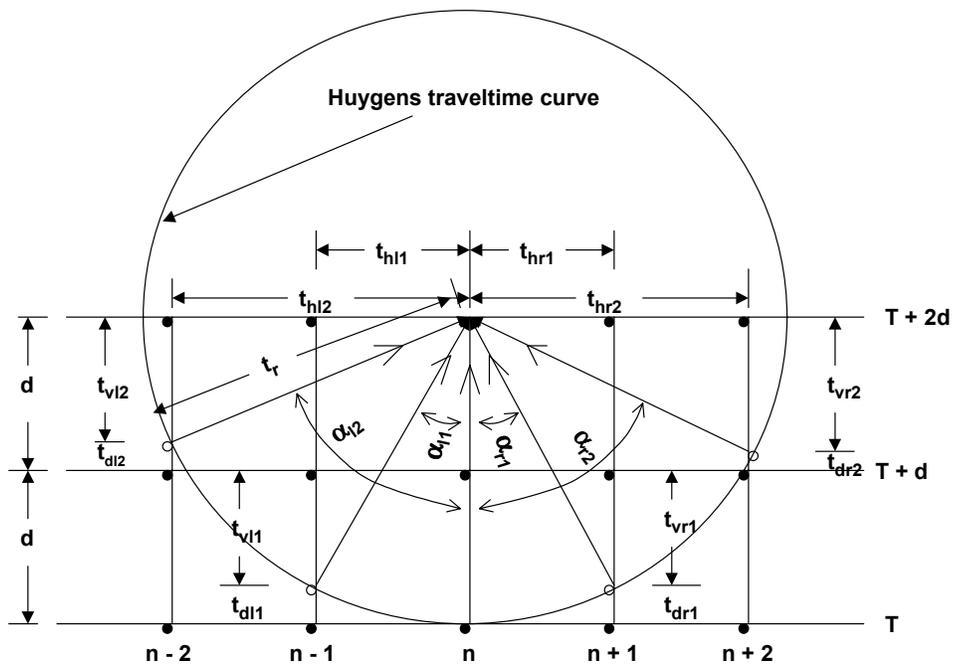


Figure 4. The various times and angles used in the five-point wavefront healing algorithm expressed in equation 2.
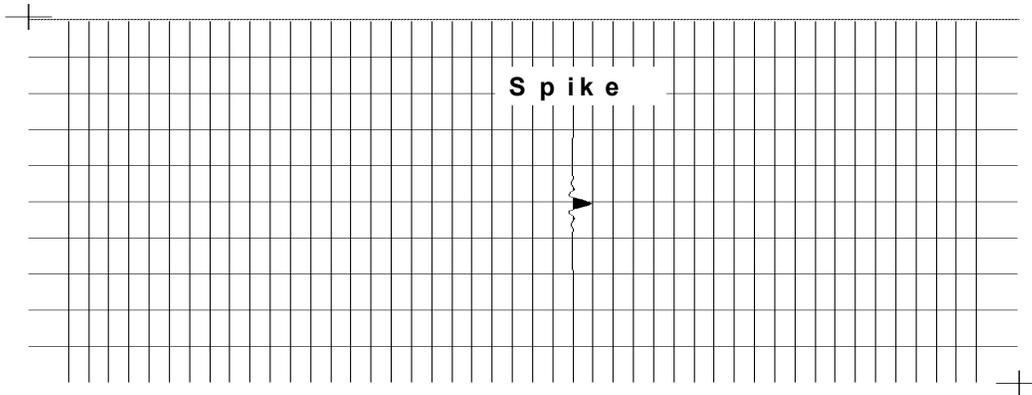
**S p i k e**

Figure 5a. Bandlimited spike to test wavefront healing algorithms

**G a p**
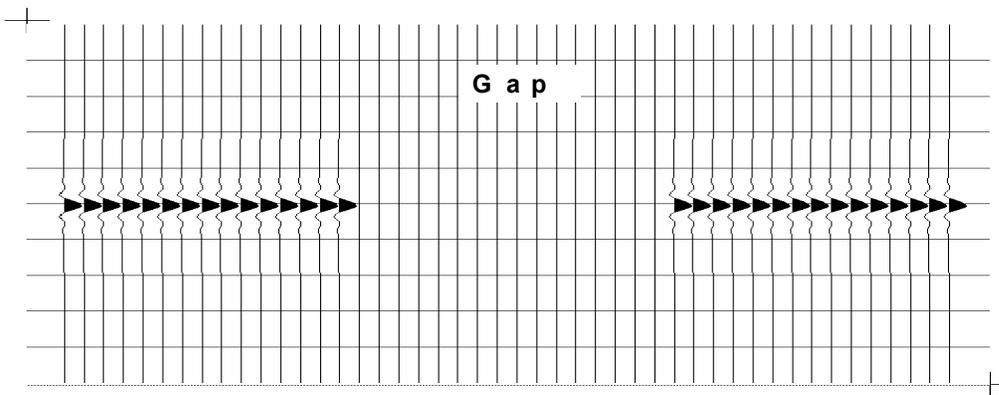
Figure 5b. Event with gap to test wavefront healing algorithms
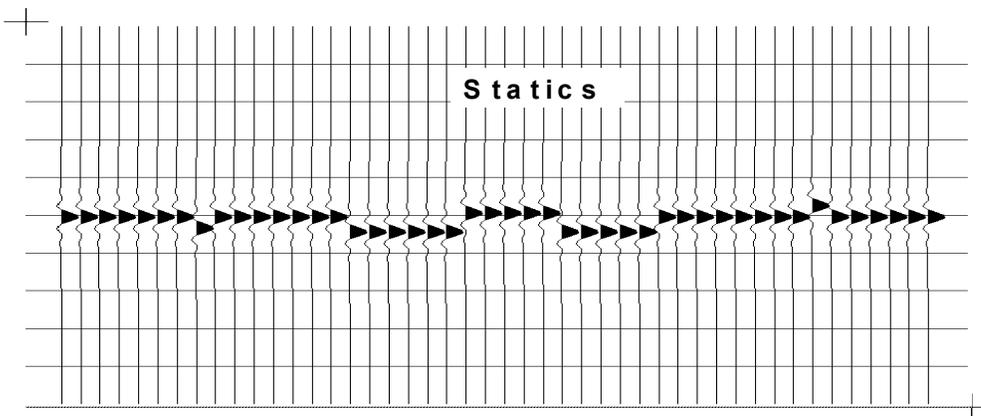
**S t a t i c s**

Figure 5c. Event with simulated statics to test wavefront healing algorithms
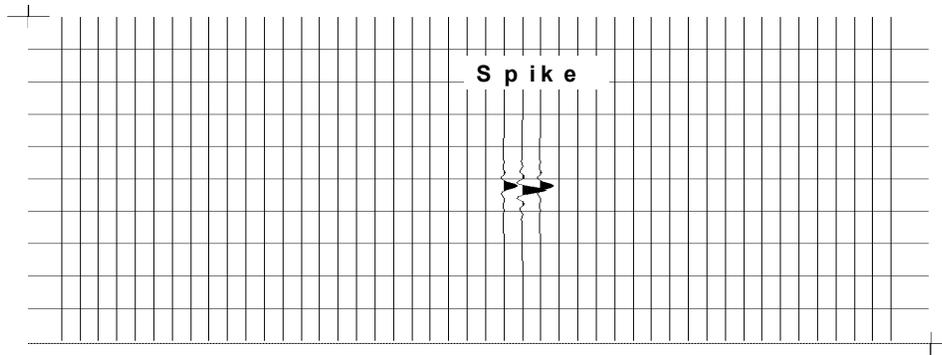
Figure 6a. Spike response of one pass of the three-point wavefront healing operator
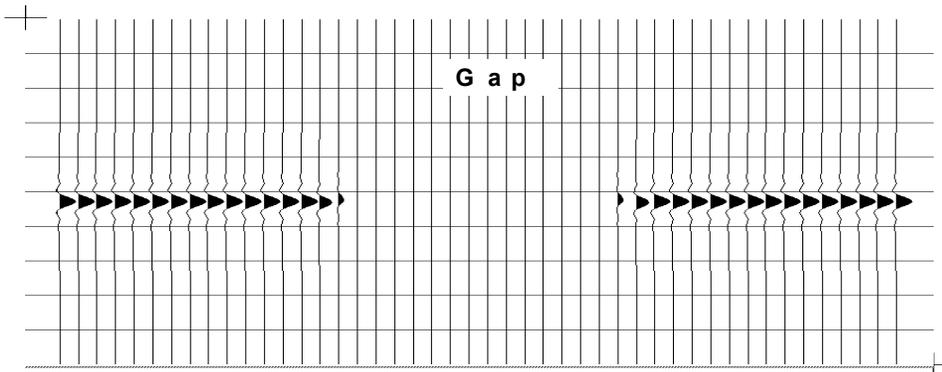
Figure 6b. Response of event with gap to three-point wavefront healing operator
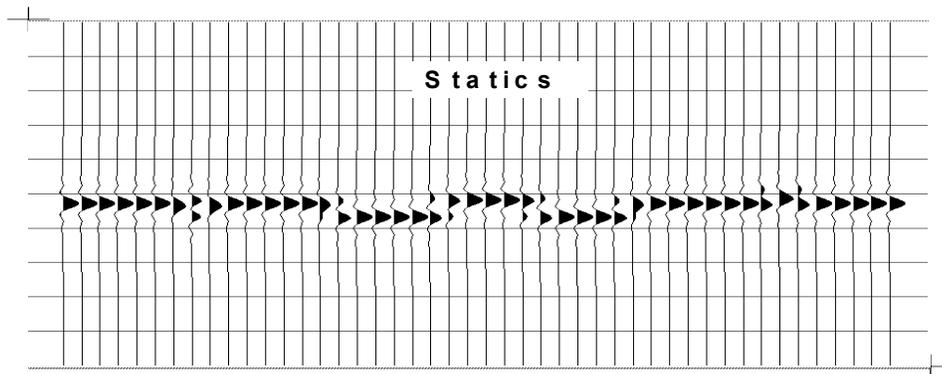
Figure 6c. Response of event with simulated statics to three-point wavefront healing operator
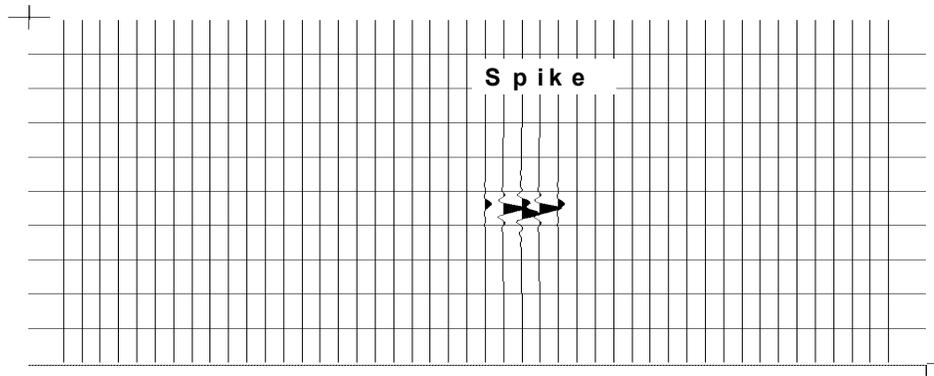
Figure 7a. Spike response to two passes of three-point wavefront healing operator
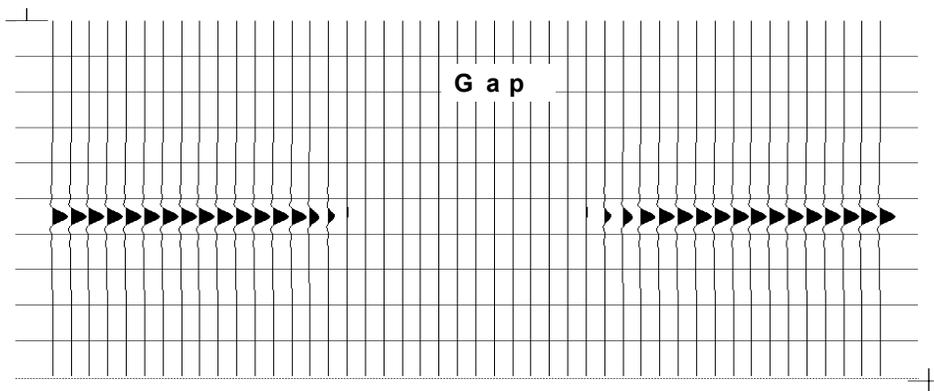


Figure 7b. Response of event with gap to two passes of three-point wavefront healing operator
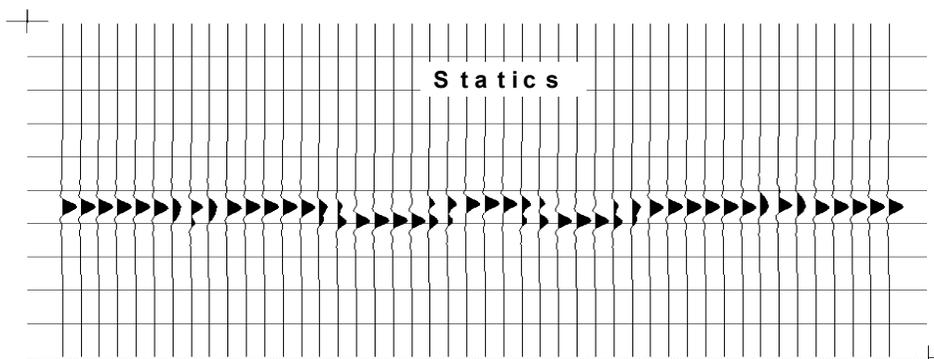


Figure 7c. Response of event with simulated statics to two passes of wavefront healing operator
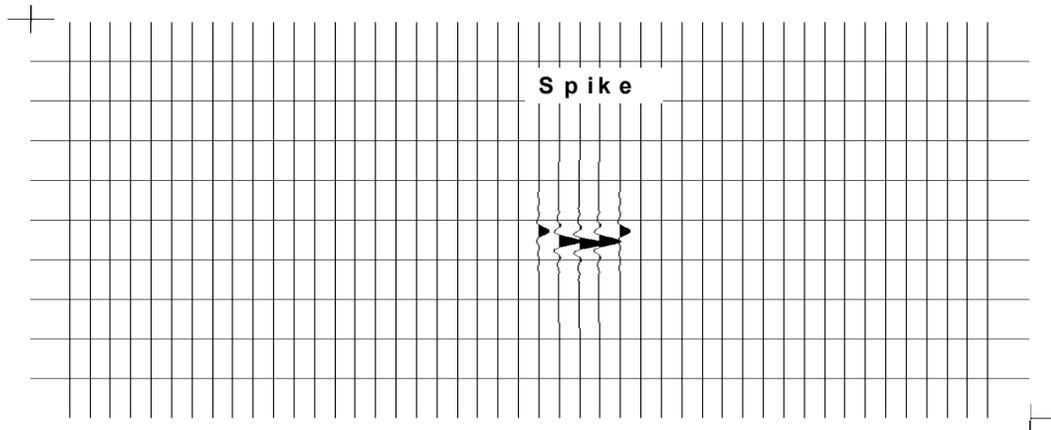
Figure 8a. Spike response to one pass of five-point wavefront healing operator
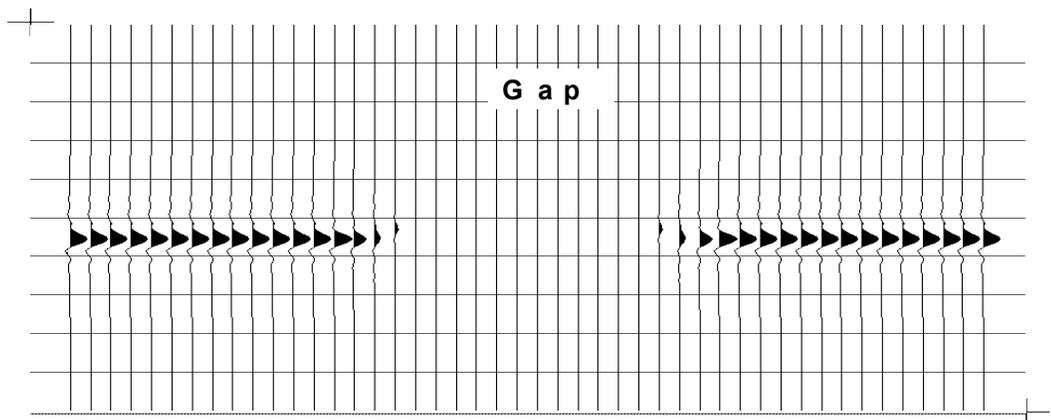


Figure 8b. Response of event with gap to one pass of five-point wavefront healing operator
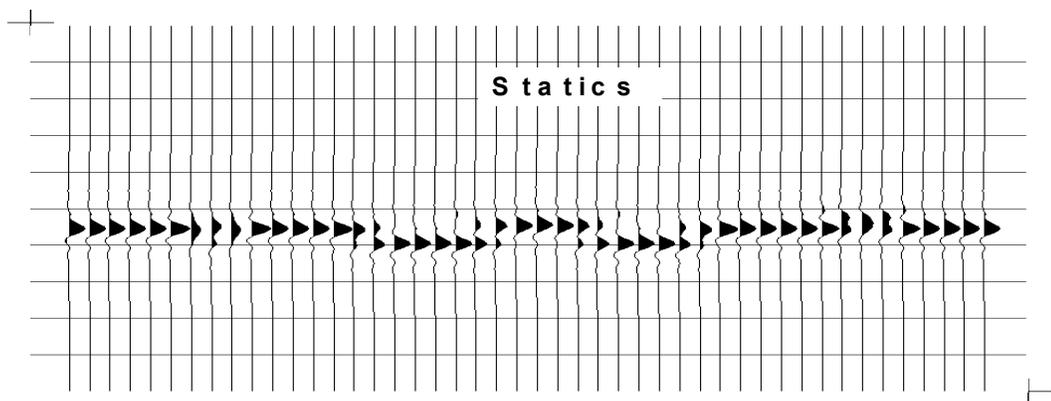


Figure 8c. Response of event with simulated statics to one pass of five-point wavefront healing operator
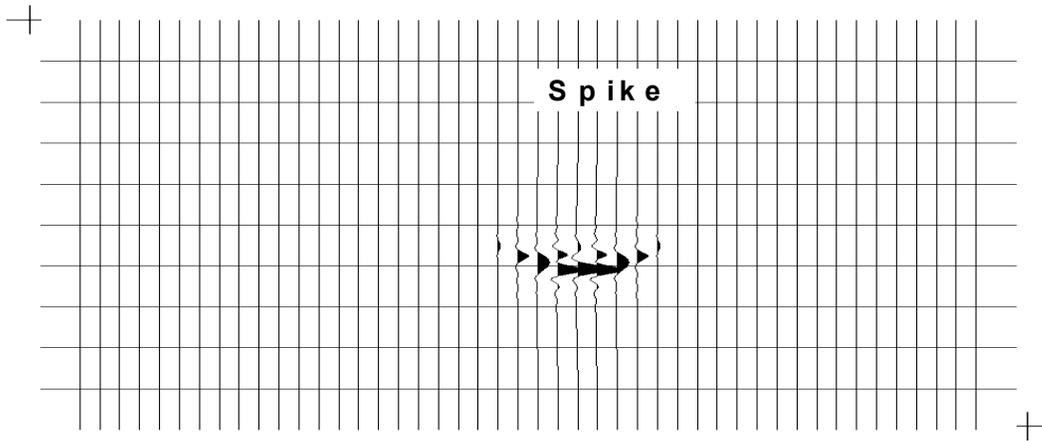
Spike

Figure 9a. Spike response to two passes of five-point wavefront healing operator

Gap
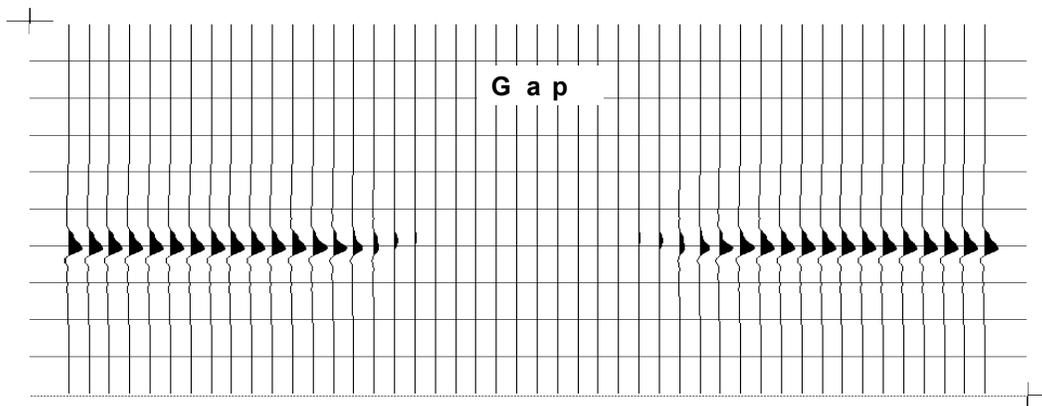
Figure 9b. Response of event with gap to two passes of five-point wavefront healing operator
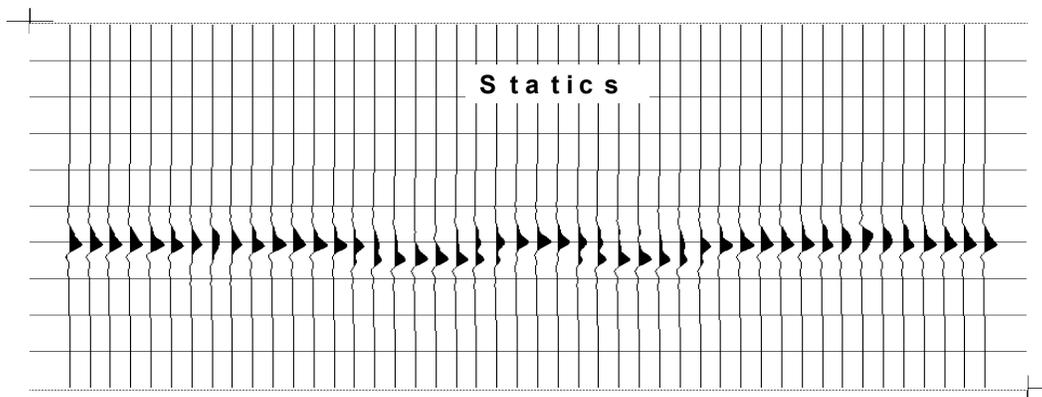
Statics

Figure 9c. Response of event with simulated statics to two passes of five-point wavefront healing operator
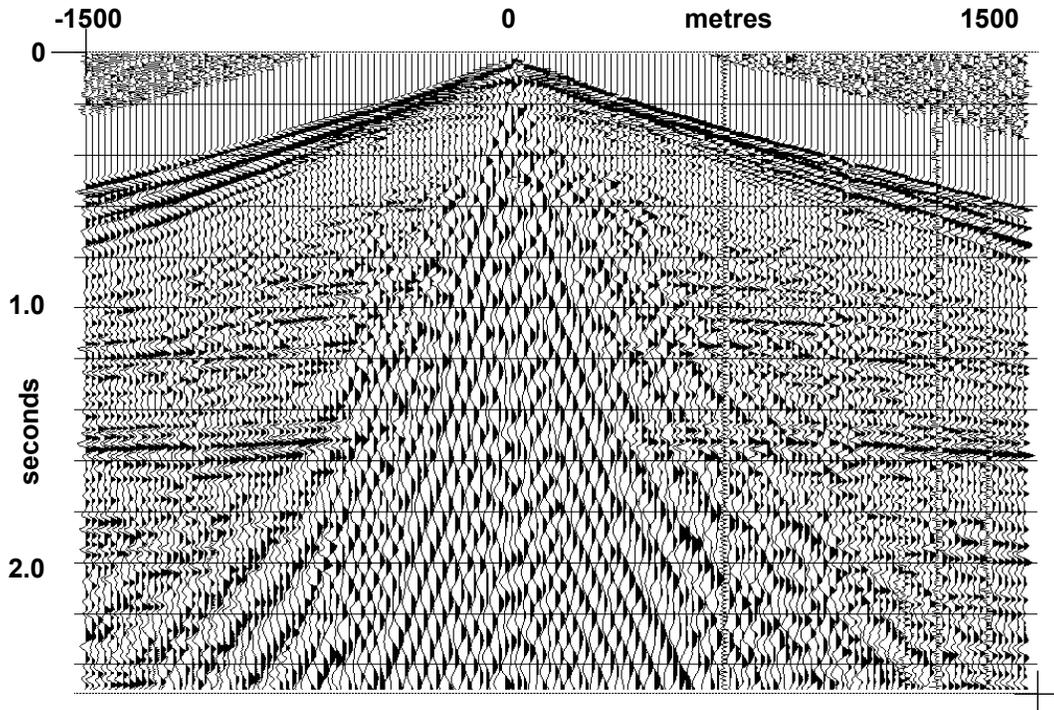
Figure 10. Raw shot gather from the Blackfoot 2-D 3-C survey used to test wavefront healing
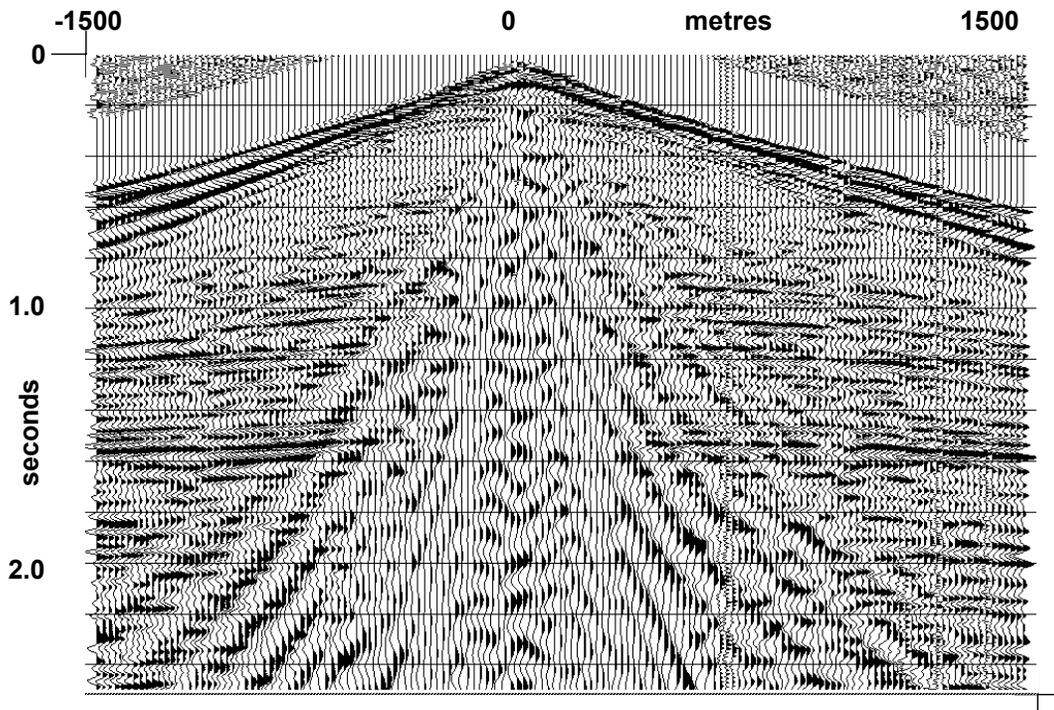


Figure 11a. Shot gather from Figure 10 after one pass of three-point wavefront healing
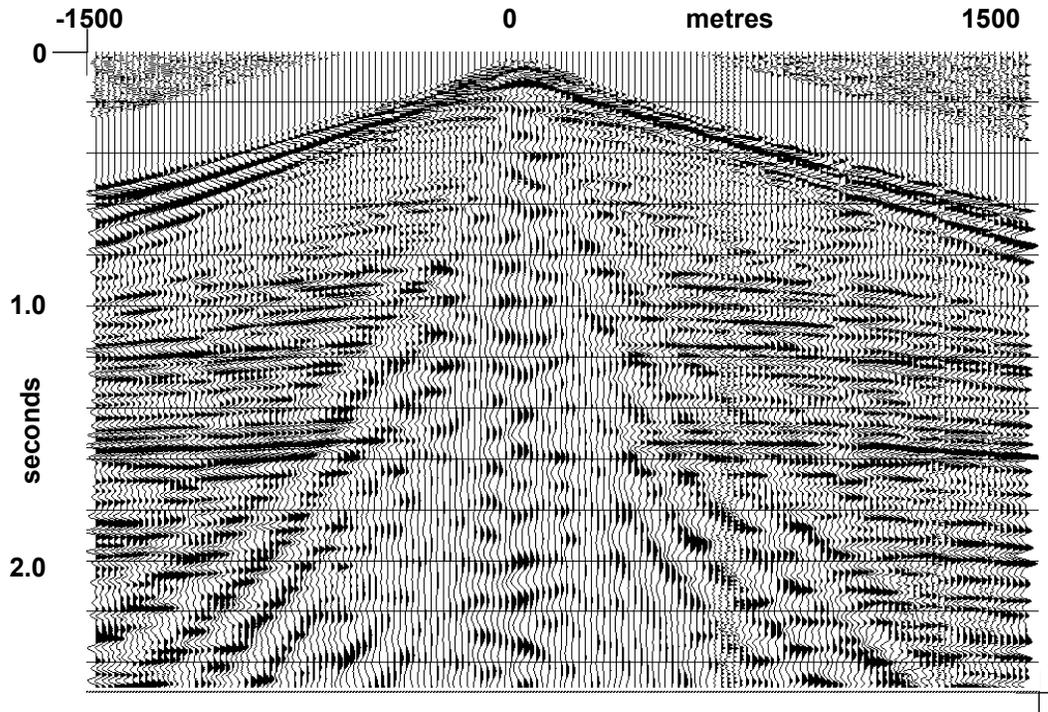
Figure 11b. Shot gather from Figure 10 after one pass of five-point wavefront healing
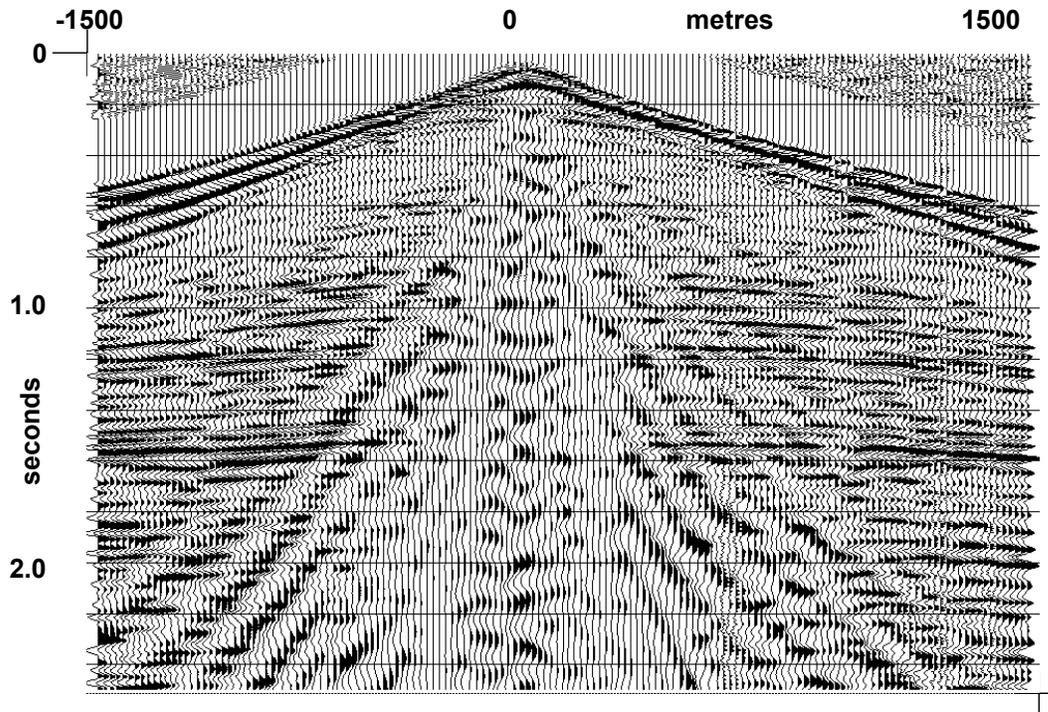


Figure 11c. Shot gather from Figure 10 after two passes of three-point wavefront healing
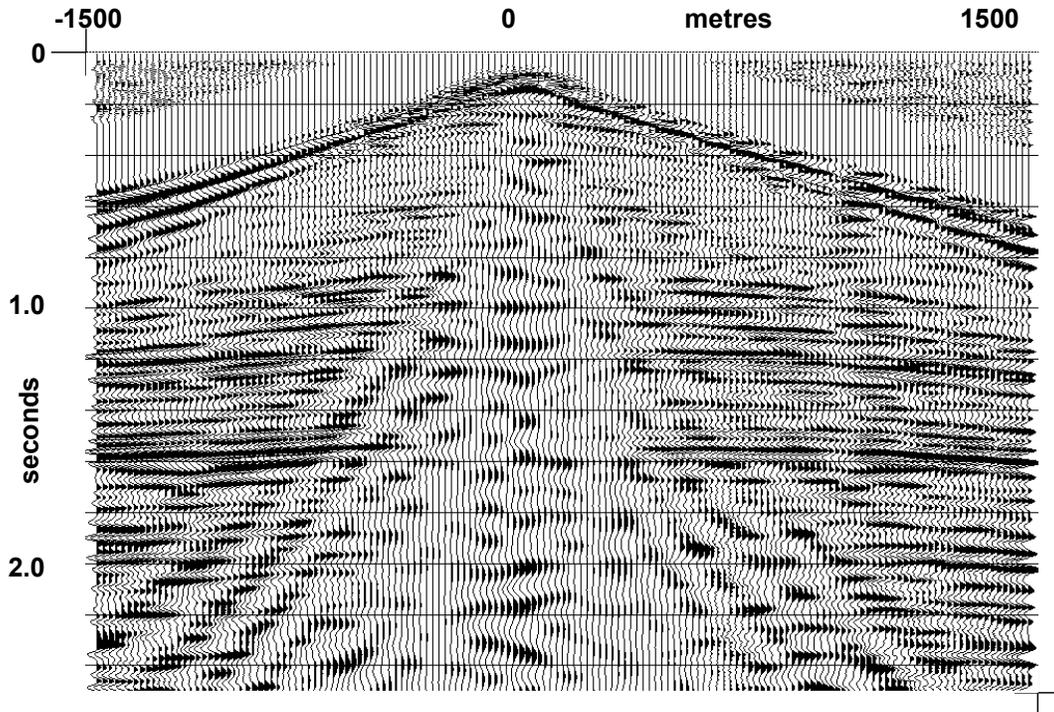
Figure 11d. Shot gather from Figure 10 after two passes of five-point wavefront healing
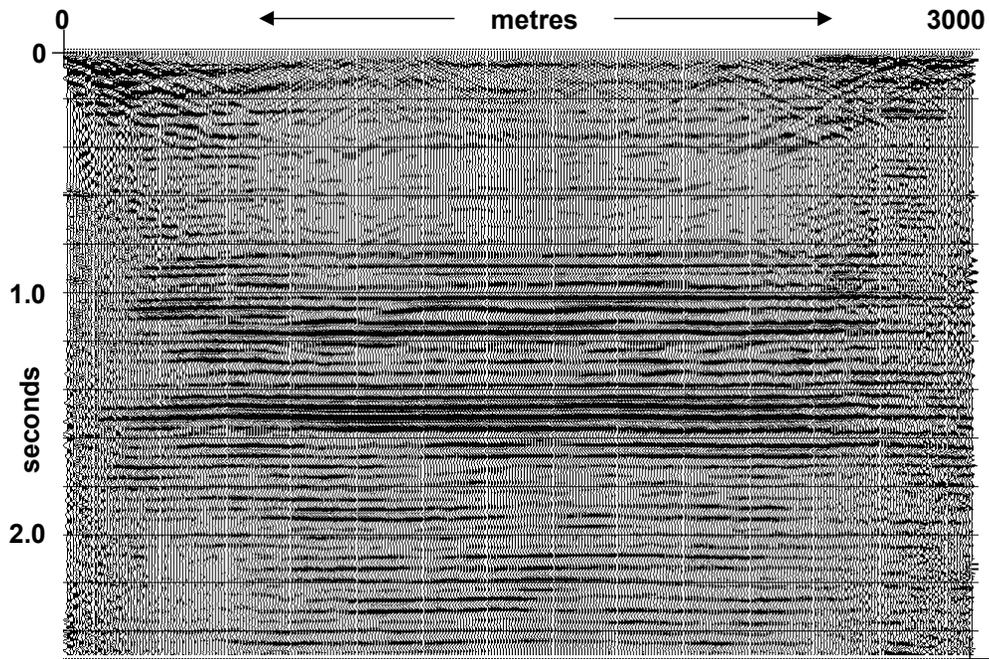


Figure 12. Brute stack of Blackfoot 2-D 3-C survey data
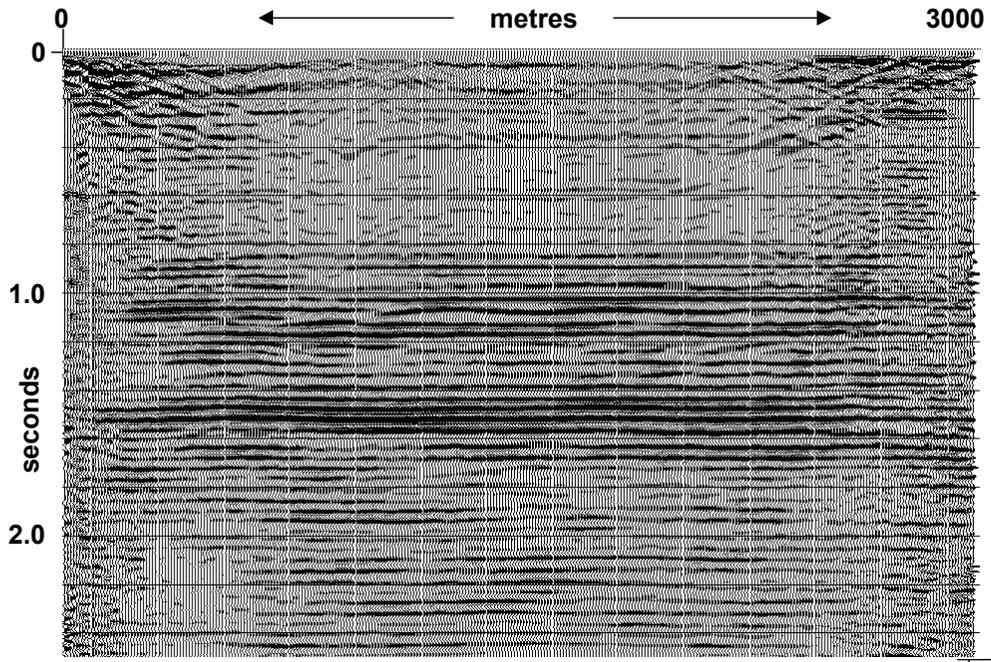
Figure 13a. Stack of Figure 12 after one pass of three-point wavefront healing
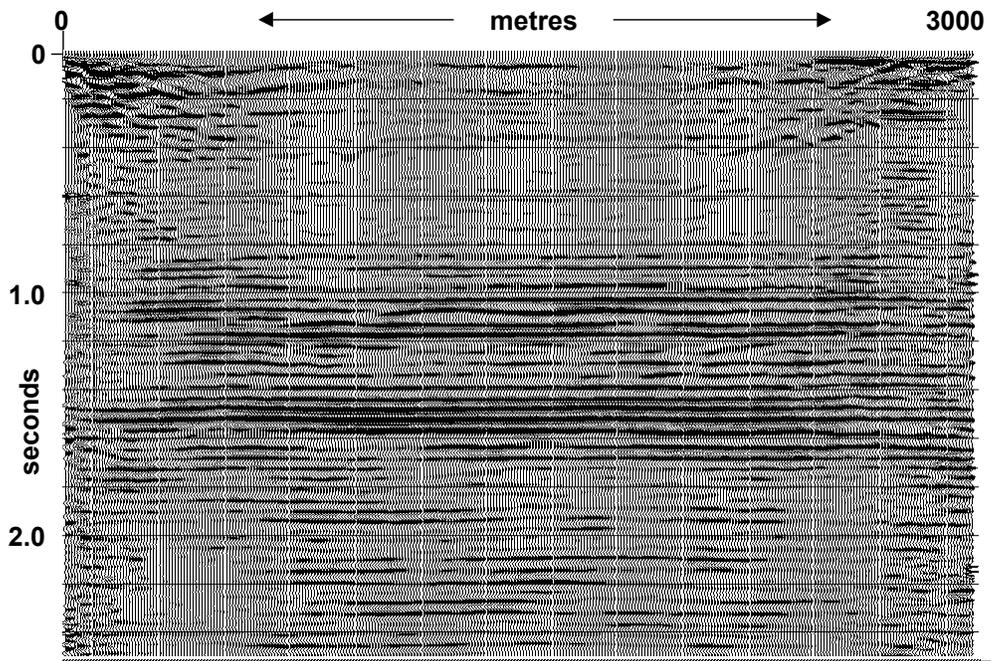


Figure 13b. Stack of Figure 12 after one pass of five-point wavefront healing